

# Importance of the Debye Screening Length on Nanowire Field Effect Transistor Sensors

Eric Stern,<sup>†</sup> Robin Wagner,<sup>†</sup> Fred J. Sigworth,<sup>†</sup> Ronald Breaker,<sup>§</sup>  
Tarek M. Fahmy,<sup>\*,†</sup> and Mark A. Reed<sup>\*,‡,||</sup>

*Departments of Biomedical Engineering, Electrical Engineering, Molecular, Cellular, and Developmental Biology and Howard Hughes Medical Institute, Applied Physics, Yale University, P.O. Box 208284, New Haven, Connecticut 06520*

*Received July 23, 2007; Revised Manuscript Received September 10, 2007*

## ABSTRACT

Nanowire field effect transistors (NW-FETs) can serve as ultrasensitive detectors for label-free reagents. The NW-FET sensing mechanism assumes a controlled modification in the local channel electric field created by the binding of charged molecules to the nanowire surface. Careful control of the solution Debye length is critical for unambiguous selective detection of macromolecules. Here we show the appropriate conditions under which the selective binding of macromolecules is accurately sensed with NW-FET sensors.

The ability to rapidly sense minute concentrations of specific macromolecules such as DNA sequences is critical for clinical diagnostics,<sup>1,2</sup> genomics,<sup>3,4</sup> and drug discovery<sup>3,4</sup> and useful for applications in defense and homeland security.<sup>5</sup> Most current systems for macromolecular sensing rely on labels, such as radiolabeled tags or fluorophores.<sup>6–8</sup> Techniques that could distinguish these without the need for labels, i.e., label-free sensing, are of great interest because they would not only significantly decrease the cost and time needed for sample preparation but would also eliminate issues related to modification of target molecules.<sup>9,10</sup>

One of the most promising platforms for unlabeled sensing is the nanowire field effect transistor (NW-FET).<sup>9–11</sup> These devices operate similarly to conventional chemical FETs, sensing the presence of bound species by their intrinsic charge, with the advantage of enhanced sensitivity due to the nanoscale channel confinement.<sup>11,12</sup> By binding a receptor protein or a single-stranded DNA (ssDNA) oligomer to the NW-FET surface, the binding of the specific ligand or complementary ssDNA modifies the electric field surrounding the device, enabling direct electronic detection.<sup>13–16</sup>

The integration issues faced by traditional, as-grown NWs have been overcome with the advent of NW-like devices patterned by “top-down” microlithography.<sup>14–18</sup> Although

early devices suffered from low signal-to-noise ratios, a “top-down” method producing high-quality nanosensors capable of detecting specific antibodies at  $\ll 10$  fM concentrations have recently been demonstrated.<sup>17</sup> In this Letter, we demonstrate the effect of molecular charge screening by dissolved solution counterions, Debye screening,<sup>19</sup> on sensor response. This is a critical consideration for designing optimal protocols for label-free sensing using NW-FETs.

The charge of solution-based molecules and macromolecules is screened by dissolved solution counterions: a negative species such as streptavidin or DNA will be surrounded by positively charged ions due to electrostatic interactions. On a certain length scale, termed the Debye length ( $\lambda_D$ ), the number of net positive charges approaches the number of negative charges on the protein or DNA. The result is a screening effect such that the electrostatic potential arising from charges on the protein or DNA decays exponentially toward zero with distance.<sup>19</sup> For aqueous solutions at room temperature, this length is given by

$$\lambda_D = \frac{1}{\sqrt{4\pi l_B \sum_i \rho_i z_i^2}} \quad (1)$$

where  $l_B$  is the Bjerrum length = 0.7 nm,  $\sum_i$  is the sum over all ion species, and  $\rho_i$  and  $z_i$  are the density and valence, respectively, of ion species  $i$  (ref 19). Thus, for optimal sensing, the Debye length must be carefully selected for NW-FET measurements because molecules binding to the devices

\* Corresponding authors. E-mail: Tarek.Fahmy@Yale.edu (T.M.F.); Mark.Reed@Yale.edu (M.A.R.).

<sup>†</sup> Department of Biomedical Engineering.

<sup>‡</sup> Departments of Electrical Engineering.

<sup>§</sup> Department of Molecular, Cellular, and Developmental Biology and Howard Hughes Medical Institute.

<sup>||</sup> Department of Applied Physics.

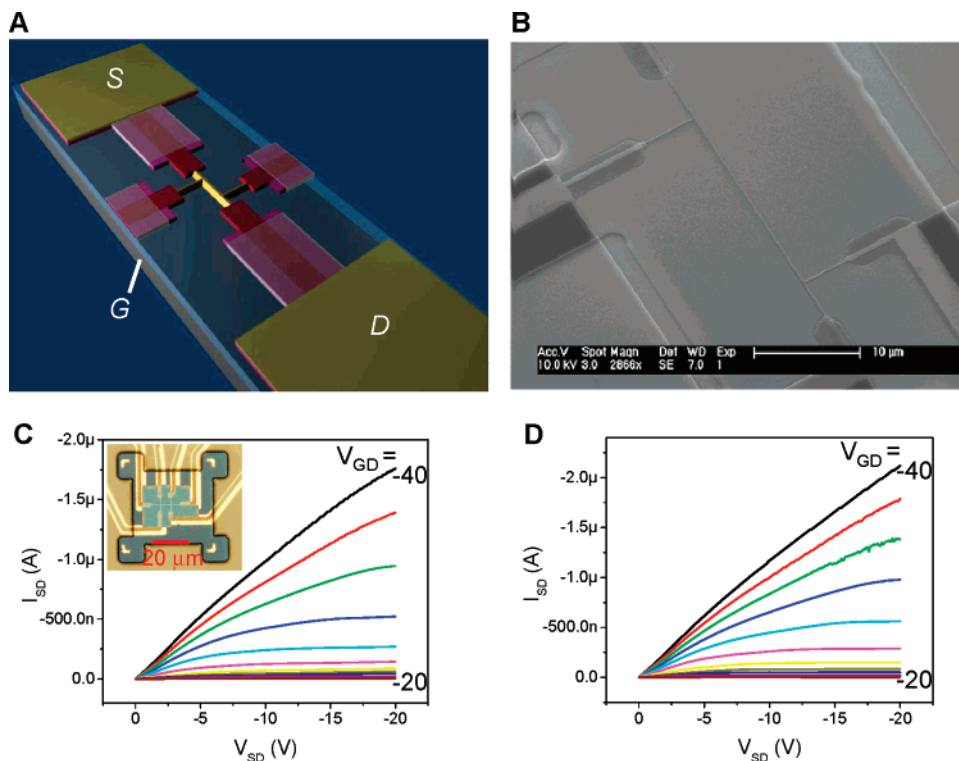


**Figure 1.** Device schematic, scanning electron micrograph, and pre- and post-functionalization transport properties. (A) Schematic (not to scale) of a completed four-point NW-FET device with source (*S*), drain (*D*), and gate (*G*) defined for the two-point sensing configuration used in this study. The active (TMAH-defined) device region is colored yellow, degenerately doped (boron) leads are red, the remainder of the active silicon layer is pink, the masking oxide is translucent and visible above the leads, contact pads are gold, the buried oxide is light blue, and the handle wafer is silver. (B) Scanning electron micrograph of a completed four-point device. The NW-FET (active device) length for the in-line leads [the configuration shown in (A)] is 30  $\mu\text{m}$ . (C and D)  $I_{\text{SD}}(V_{\text{SD}})$  dependence for  $V_{\text{GD}}$  varied in  $-2$  V steps for a representative device in air (C) before and (D) after functionalization with APTS. The inset in (C) is an optical micrograph of a representative device. Hardbaked photoresist coats the die surface area except above the device.

are removed from the sensor surface by  $\sim 2\text{--}12$  nm (the size of the receptor proteins or DNA linkers bound to the sensor surface).

Nanowire-FET devices were fabricated from silicon-on-insulator (SOI) wafers as described previously in ref 17. Briefly, the NW-FET device regions were defined with a wet chemical etch (tetramethylammonium hydroxide, TMAH), which etches Si(111) planes at  $\sim 1/100$  the rate of all other planes and thereby eliminates edge imperfections not aligned to this plane. Electron-beam lithography and subsequent reactive-ion etching were used to define the device dimensions in a thermally grown masking oxide, and TMAH etching was subsequently used to transfer the pattern to the active silicon layer. It should be noted that this etch produces trapezoidal devices due to the (100) orientation of the SOI wafers. As illustrated in the schematic in Figure 1A, the etching causes undercutting of the masking oxide into the lightly doped (boron,  $10^{15}\text{ cm}^{-3}$ ) region (yellow), which in turn allows the realization of devices with significantly smaller dimensions than originally defined. The doped source and drain contacts (dark red, degenerately doped to  $>10^{20}\text{ cm}^{-3}$  with boron by ion implantation) extend under the metal contact pads and are not appreciably etched by the TMAH. A scanning electron micrograph of a representative NW-FET device is shown in Figure 1B. Four-point measurements showed that the devices had negligible contact resistance,

and all sensing measurements were therefore taken in a two-point configuration as depicted in Figure 1A.

We studied the transport characteristics of a device before and after surface functionalization because surface chemistry has previously been shown to have a deleterious effect on device properties.<sup>17</sup> The dependence of source–drain current ( $I_{\text{SD}}$ ) on source–drain voltage ( $V_{\text{SD}}$ ) for varying gate–drain voltage ( $V_{\text{GD}}$ ) for a representative device is shown in Figure 1C. The large  $|V_{\text{GD}}|$  required to turn on the device is consistent with SOI accumulation-mode operation. Device functionalization with 3-aminopropyltriethoxysilane (APTS)<sup>22</sup> to convert silanol (Si–OH) groups to free amines did not significantly affect the  $I_{\text{SD}}(V_{\text{SD}})$  of the device (Figure 1D). The trivial increase in  $I_{\text{SD}}$  for large  $|V_{\text{GD}}|$  suggests the presence of a small parallel current path through the surface. This path does not appreciably contribute when the device is fully depleted ( $V_{\text{GD}} \geq -20$  V), as was the case for similar devices functionalized with dec-9-enyl-carbamic acid *tert*-butyl ester.<sup>17,21</sup> All sensing measurements in this work were DC and used  $V_{\text{SD}} = -2$  V and  $V_{\text{GD}} = -35$  V.

Functionalization with APTS produced working devices with amine-modified surfaces in high yield ( $>90\%$ ). The potential shortcoming of the APTS technique is that all exposed oxide surfaces, essentially the entire die surface area including the NW-FET, would be functionalized with amines,<sup>24</sup> thus dramatically decreasing sensitivity. We miti-

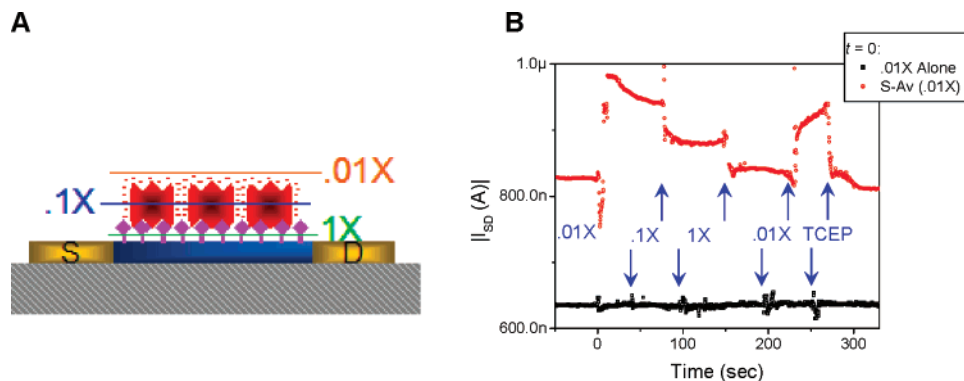


**Figure 2.** Impact of Debye screening on streptavidin sensing. (A) Schematic (not to scale) showing  $\lambda_D$  from the device surface. The blue bar represents the active region of the device, the yellow regions the leads ( $S =$  source,  $D =$  drain), the gray hashed region the underlying oxide, the purple diamonds are biotin, and the red objects are streptavidin. The negative charges surrounding the protein represent its negative charge. The green “1×” line (also not to scale) represents the screening length ( $\lambda_D$ ) from 1× PBS relative to the protein and the blue and orange lines represent that from 1:10 and 1:100 dilutions of this buffer, respectively. (B) Biotin-functionalized sensor response ( $|I_{SD}|$  vs time) to varying buffer ionic concentrations with (red) and without (black) streptavidin addition at  $time = 0$ . The blue text gives the PBS buffer concentration [Tris(2-carboxyethyl)phosphine hydrochloride, TCEP, was added in 0.01× PBS] and the blue arrows represent the onset of solution exchange. The two results derive from different devices.

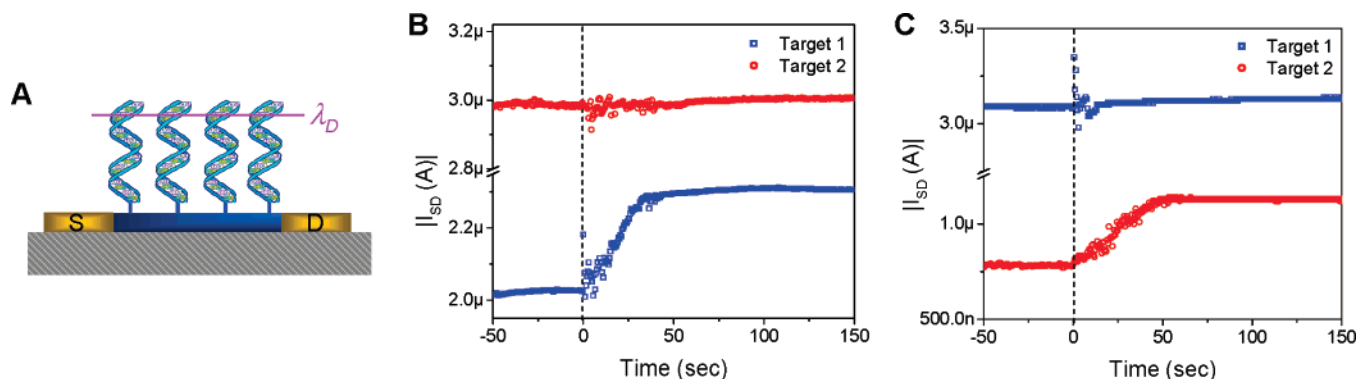


**Figure 3.** Specific detection of unlabeled ssDNA. (A) Schematic (not to scale) showing  $\lambda_D$  ( $\sim 3.3$  nm) from the device surface. Unbound target DNA strands will be screened, while the majority of the charge of hybridized strands will not. (B,C) Response of NW-FETs functionalized with the (B) probe 1 and (C) probe 2 DNA strands to the addition of 10 pM solutions of target DNA strands. Solution exchange occurs at  $time = 0$ , highlighted by the dashed line.

gated this problem by patterning a final photoresist layer that exposed only a small region around the active devices (inset, Figure 1A).<sup>25</sup>

We first demonstrate the effect of increasing buffer ionic strengths (decreasing  $\lambda_D$ ) on device sensitivity for recognition.<sup>19</sup> For these studies, we chose the well-studied biotin–streptavidin ligand–receptor system,<sup>17,23</sup> which is known to be unaffected by variations in buffer salt concentrations.<sup>23,26</sup> A NW-FET device was functionalized with a cleavable biotin molecule<sup>27</sup> and, after establishing a baseline current in 0.01× PBS, 10 nM streptavidin was added in the same buffer. The binding of streptavidin, a negative protein with an isoelectric point (pI) of  $\sim 5.6$  (ref 17), to the biotinylated device resulted in an increased  $|I_{SD}|$  of the p-type device (Figure 2B). The ionic strength of this buffer yields a  $\lambda_D$  of  $\sim 7.3$  nm. Thus the majority of the protein’s charge is unscreened at the NW-FET surface (Figure 2). A 10-fold increase in the ionic strength of the buffer (0.1× PBS,  $\lambda_D \sim 2.3$  nm) partially screens streptavidin’s intrinsic charge, and a further 10-fold increase in buffer ionic strength (1× PBS,  $\lambda_D \sim 0.7$  nm) effectively screens most of the protein’s charge, returning

the  $|I_{SD}|$  approximately to its baseline value (Figure 2B). The device current level begins to recover to its 0.01× PBS value after a subsequent decrease in ionic strength by solution exchange with this buffer. The addition of the reducing agent tris(2-carboxyethyl)phosphine hydrochloride (TCEP), which cleaves the biotin linker<sup>17,23</sup> and thus removes streptavidin from the sensor surface, returns  $|I_{SD}|$  to its original, baseline level, Figure 2B (see also Supporting Information Figure 2). As a control, the same series of solution exchanges was applied to a nominally identical biotinylated device using streptavidin-free buffers (Figure 2B). The absence of a change in signal demonstrates that the NW-FET response is independent of ionic strength (e.g.,  $\lambda_D$ ). It is important to note that the negligible changes in NW-FET current upon buffer exchanges in the streptavidin-free control also serves to demonstrate that the buffer pH’s are the same because previous work demonstrated the sensitivity of these devices to pH changes.<sup>17</sup>

Device utility for specific ssDNA strand recognition was demonstrated by performing a cross-comparison assay. Two devices were functionalized with the DNA-probe(1) [P(1)]

sequence and two others with the DNA-P(2) sequence.<sup>28,29</sup> Under active measurement conditions ( $V_{SD} = -2$  V,  $V_{GD} = -35$  V) and after the establishment of a baseline signal in  $0.05 \times$  PBS, the solution was exchanged with 10 pM solutions of target DNA, either DNA-T(1) or DNA-T(2), in the same buffer.<sup>28</sup> The schematic in Figure 3A illustrates the Debye length relative to the NW-FET sensor surface. Bound strands lie within  $\lambda_D$ , while unbound strands are screened. Panels B and C of Figure 3 show the responses of the DNA-P(1)- and DNA-P(2)-functionalized devices, respectively, to DNA-T(1) and DNA-T(2). In both cases, complementary pairing results in an increase in  $|I_{SD}|$ , as expected for a p-type device, while the noncomplementary negative controls show little change in signal, indicating that we have chosen a buffer with an optimal  $\lambda_D$ . The negligible signal of the negative controls indicates that our choice of  $\lambda_D \sim 3.3$  nm effectively screens unbound DNA. [A similar set of experiments performed using buffers with significantly greater Debye screening lengths (much lower ion concentrations) gave false positives.] These data are consistent with a conventional fluorescence-microscopy-based labeled-DNA assay performed with the same surface chemistry on glass slides (Supporting Information Figure 3).

By using a previously described<sup>17</sup> analyte fluid introduction procedure in which the velocity of injected solutions is tangential to the NW-FET sensor, we have obtained significantly faster detection response times than those observed in NW-FET studies that use microchannels for target DNA delivery.<sup>13,16</sup> As described in ref 30, the use of microchannels severely restricts the ability of molecules to reach the nanosensor surface because flow is strictly laminar in such channels and, in turn, molecular transport only occurs via diffusion. Thus, the nanosensor response time is limited by the microfluidics and not by the NW-FET itself. By overcoming this limitation, we are able to achieve complete 20-mer hybridization after 35–50 s, a response time significantly faster than that observed previously.<sup>13,16</sup>

Our results demonstrate the importance of selecting a buffer with an appropriate  $\lambda_D$  to ensure proper NW-FET sensing. Careful control of the solution Debye length ensures that specific binding of macromolecules contribute to sensor response. An autonomous system for analyte detection must properly take these issues into account such as employing ionic strength feedback control. This demonstration also profiles an application where charge distribution may enable unique measurements of the configuration of surface-bound species.

**Acknowledgment.** We thank R. Ilic, D. Westly, M. Metzler, and V. Genova of the Cornell Nanofabrication Facility for device processing assistance, D. Routenberg, G. Cheng, J. Hyland, M. Young, and C. Tillinghast for helpful device processing discussions, and D. Stern for sensing discussions and assistance in manuscript preparation. This work was partially supported by DARPA through ONR and AFOSR, NASA, ARO, the Coulter Foundation, by a Department of Homeland Security graduate fellowship, and by a NSF graduate fellowship. This work was performed in part at the Cornell Nanoscale Science and Technology Facility,

a member of the National Nanotechnology Infrastructure Network that is supported by the NSF.

**Supporting Information Available:** Figures demonstrating device stability and response to changes in pH and a labeled DNA assay. This material is available free of charge via the Internet at <http://pubs.acs.org>.

## References

- (1) Ligler, F. S.; Erickson, J. S. *Nature* **2006**, *440*, 159–160.
- (2) Dawson, E. D.; Moore, C. L.; Dankbar, D. M.; Mehlmann, M.; Townsend, M. B.; Smagala, J. A.; Smith, C. B.; Cox, N. J.; Kuchta, R. D.; Rowlen, K. L. *Anal. Chem.* **2007**, *79*, 378–384.
- (3) Cretich, M.; Damin, F.; Pirri, G.; Chiari, M. *Biomol. Eng.* **2006**, *23*, 77–88.
- (4) Janasek, D.; Franzke, J.; Manz, A. *Nature* **2006**, *442*, 374–380.
- (5) Lim, D. V.; Simpson, J. M.; Kearns, E. A.; Kramer, M. F. *Clin. Microbiol. Rev.* **2005**, *18*, 583–607.
- (6) Crowther, J. R. *ELISA: Theory and Practice*; Humana Press: New York, 1995.
- (7) Kricka, L. J. *Nonisotopic Probing, Blotting, and Sequencing*, 2nd ed.; Academic Press: New York, 1995.
- (8) Madou, M. J.; Cubicciotti, R. *Proc. IEEE* **2003**, *91*, 830–838.
- (9) Ramachandran, N.; Larson, D. N.; Stark, P. R. H.; Hainsworth, E.; LaBaer, J. *FEBS J.* **2005**, *272*, 5412–5425.
- (10) Cheng, M. M.-C.; Cuda, G.; Bunimovich, Y. L.; Gaspari, M.; Heath, J. R.; Hill, H. D.; Mirkin, C. A.; Nijdam, A. J.; Terracciano, R.; Thundat, T.; Ferrari, M. *Curr. Opin. Chem. Biol.* **2006**, *10*, 11–19.
- (11) Patolsky, F.; Zheng, G.; Lieber, C. M. *Nanomedicine* **2006**, *1*, 51–65.
- (12) Klemic, J. F.; Stern, E.; Reed, M. A. *Nat. Biotechnol.* **2001**, *19*, 924–925.
- (13) Hahn, J.-i.; Lieber, C. M. *Nano Lett.* **2004**, *4*, 51–54.
- (14) Li, Z.; Chen, Y.; Li, X.; Kamins, T. I.; Nauka, K.; Williams, R. S. *Nano Lett.* **2004**, *4*, 245–247.
- (15) Fritz, J.; Cooper, E. B.; Gaudet, S.; Sorger, P. K.; Manalis, S. R. *Proc. Natl. Acad. Sci. U.S.A.* **2002**, *99*, 14142–14146.
- (16) Bunimovich, Y.; Shin, Y. S.; Yeo, W.-S.; Amori, M.; Kwong, G.; Heath, J. R. *J. Am. Chem. Soc.* **2006**, *128*, 16323–16331.
- (17) Stern, E.; Klemic, J. F.; Routenberg, D. A.; Wyrembak, P. N.; Turner-Evans, D. B.; Hamilton, A. D.; LaVan, D. A.; Fahmy, T. M.; Reed, M. A. *Nature* **2007**, *445*, 519–522.
- (18) Gao, Z.; Agarwal, A.; Trigg, A. D.; Singh, N.; Fang, C.; Tung, C.-H.; Fan, Y.; Buddharaju, K. D.; Kong, J. *Anal. Chem.* **2007**, *79*, 3291–3297.
- (19) Israelachvili, J. *Intermolecular & Surface Forces*, 2nd Ed.; Academic Press: London, 1991.
- (20) Gupta, A. K.; Nair, P. R.; Akin, D.; Ladisch, M. R.; Broyles, S.; Alam, M. A.; Bashir, R. *Proc. Natl. Acad. Sci. U.S.A.* **2006**, *103*, 13362–13367.
- (21) Streifer, J. A.; Kim, H.; Nichols, B. M.; Hamers, R. J. *Nanotechnology* **2005**, *16*, 1868–1873.
- (22) APTS functionalization: Devices were treated with a 1% (w/v) solution of APTS in hexanes with shaking for 1.5 h. The devices were then rinsed in hexanes and toluene, followed by a 10 min wash in chloroform with shaking. The devices were then rinsed with isopropanol and dried with nitrogen.
- (23) Hermanson, G. T. *Bioconjugate Techniques*; Elsevier Science & Technology Books: New York, 1996.
- (24) The NW-FET surface area is  $\sim 10^6$ -fold less than that of the entire die, potentially decreasing the sensitivity of the system by at least  $10^6$  due to binding competition.
- (25) Contact lithography was performed to pattern AZ5218-E inverting resist. After development, the resist was hardbaked at 140 °C for 1 h. This treatment enabled APTS functionalization after resist patterning; however, chlorobenzene washes longer than 10 min tended to crack the resist. Additionally, this organic layer prevented solution-induced device failure<sup>17</sup> by eliminating leakage paths to the back gate; devices on protected chips are stable in solution for >1 h (Supporting Information Figure 1).
- (26) Ross, S. E.; Carson, S. D.; Fink, L. M. *BioTechniques* **1986**, *4*, 350–354.
- (27) Sulfo-succinimidyl 2-(biotinamido)-ethyl-1,3-dithiopropionate (sulfo-NHS-SS-biotin), Pierce Co. Amine-modified surfaces were treated with sulfo-NHS-SS-biotin for 1 h at pH 8.4 with agitation.

- (28) DNA sequences: DNA-T(1): 5'-CCT GCA GTG ACG CAG TGG CG -3'; DNA-T(2): 5'-AAG GTG GAA AAT GTA ATC TA-3'; DNA-P(1): 5'-CGC CAC TGC GTC ACT GCA GG-3'; DNA-P(2): 5'-TAG ATT ACA TTT TCC ACC TT-3'.
- (29) Amine-modified surfaces were treated with sulfo-SMCC [sulfosuccinimidyl 4-(*N*-maleimidomethyl)cyclohexane-1-carboxylate], a

- heterobifunctional cross-linker, for 1 h with shaking at pH 8.5. This reaction conferred maleimide functionality to the surface. The chips were then rinsed in DI and used immediately for thiol-terminated DNA conjugation (1 h in PBS).
- (30) Sheehan, P. E.; Whitman, L. J. *Nano Lett.* **2005**, *5*, 803–807. NL071792Z